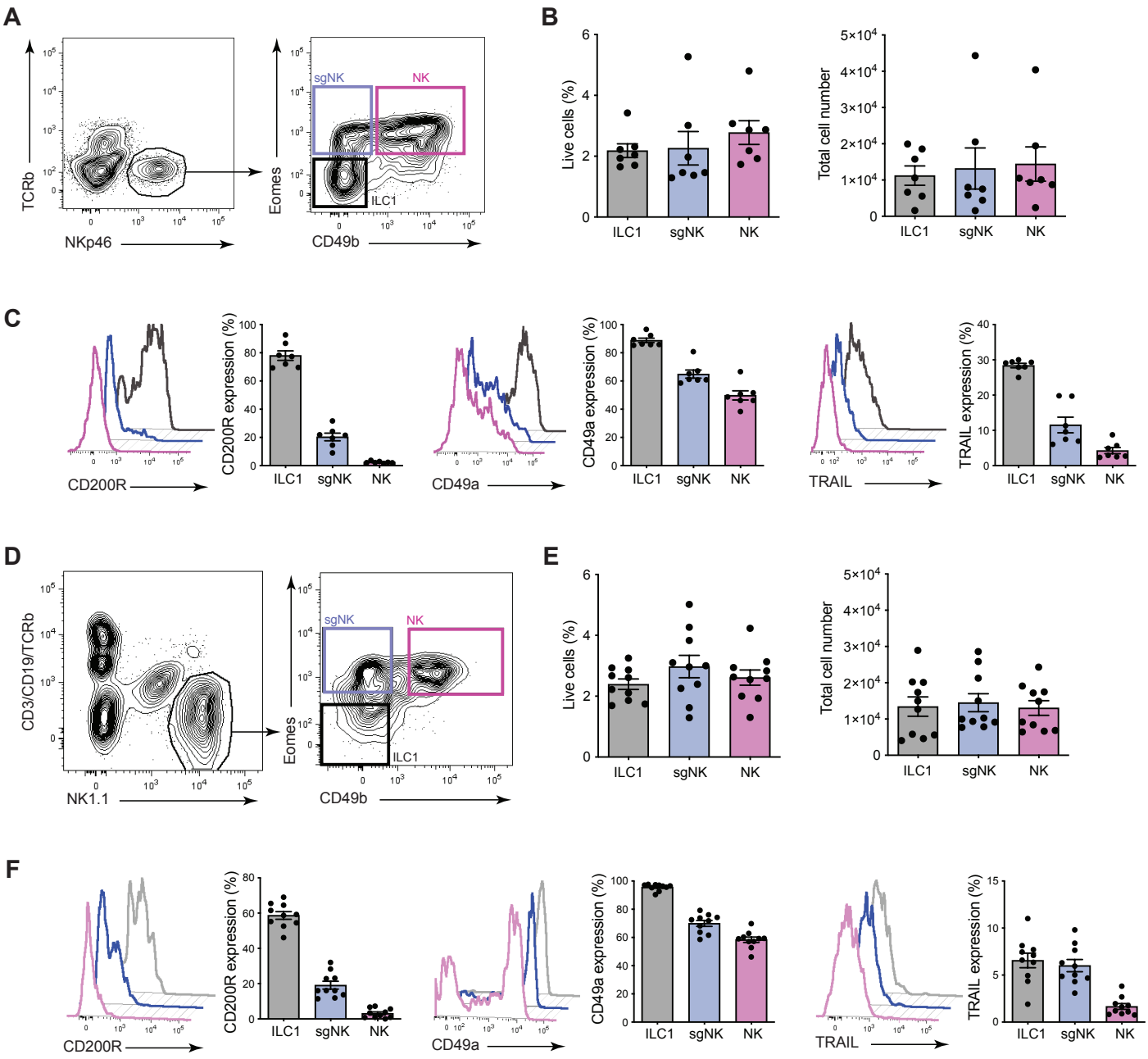

Figure S1. Three phenotypically distinct populations of group 1 ILC are present in the SG at steady state. Related to Figure 1.

Flow cytometric analysis of lymphocytes in the SG of naïve BALB/c (**A** - **C**) and C57BL/6J (**D** – **F**) mice. Representative plots of Lin$^-$ (CD19$^-$, TCRb$^-$) (**A**) NKp46 or (**D**) NK1.1 expressing cells. Eomes and CD49b expression distinguish 3 subsets: ILC1 (Eomes$^-$ CD49b$^-$), sgNK (Eomes$^+$CD49b$^-$) and NK cell (Eomes$^+$CD49b$^+$) subsets. Frequency and total number of each subset in (**B**) BALB/c and (**E**) C57BL/6J mice. Expression of CD200R, CD49a and TRAIL on ILC1, sgNK and NK cells of (**C**) BALB/c and (**F**) C57BL/6J mice. n = 9 per mouse strain pooled from 2 independent experiments. Data plotted as mean ± SEM.

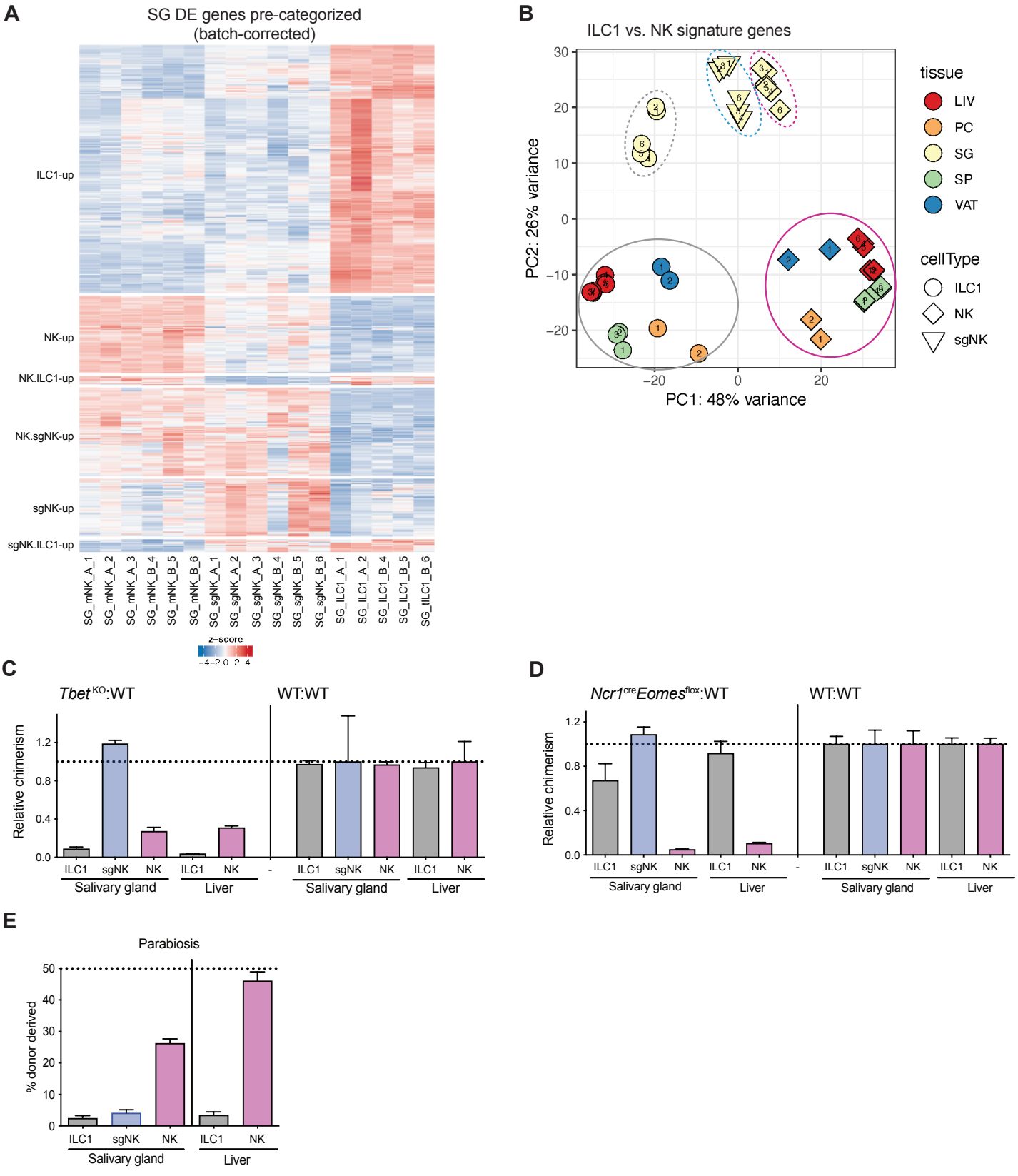
A
SG DE genes pre-categorized
(batch-corrected)
ILC1-up
NK-up
NK.ILC1-up
NK.sgNK-up
sgNK-up
sgNK.ILC1-up
SG_mNK_A_1
SG_mNK_A_2
SG_mNK_A_3
SG_mNK_B_4
SG_mNK_B_5
SG_mNK_B_6
SG_sgNK_A_1
SG_sgNK_A_2
SG_sgNK_A_3
SG_sgNK_B_4
SG_sgNK_B_5
SG_sgNK_B_6
SG_ILC1_A_1
SG_ILC1_A_2
SG_ILC1_B_4
SG_ILC1_B_5
SG_tILC1_B_6
z-score
−4 −2 0 2 4
B
ILC1 vs. NK signature genes
PC2: 26% variance
PC1: 48% variance
tissue
LIV
PC
SG
SP
VAT
cellType
ILC1
NK
sgNK
C
Tbet KO:WT
WT:WT
Relative chimerism
ILC1
sgNK
NK
Salivary gland
Liver
D
Ncr1 cre Eomes flox:WT
WT:WT
Relative chimerism
Salivary gland
Liver
E
Parabiosis
% donor derived
Salivary gland
Liver

Figure S2. SG ILC1 and NK cell populations have distinct transcriptional profiles, transcription factor-dependency and tissue residency at steady state. Related to Figure 1.

Bulk RNAseq analysis of ILC1 (CD49b^{-}Eomes^{-}), sgNK (CD49b^{-}Eomes^{+}) and NK cells (CD49b^{+}Eomes^{+}) sorted from naive B6.*Eomes*-GFP mice. (**A**) Heat map of differentially expressed genes that represent signatures for NK, ILC1 and sgNK depicts the differences and similarities within the 3 populations. Each cluster shows genes that are upregulated in one or two populations as indicated on the left. (**B**) Principal Component Analysis (PCA) of ILC1/NK cell transcriptional profiles from cells in liver (LIV, n = 6), spleen (SP, n = 5), peritoneal cavity (PC n = 2) and visceral adipose tissue (VAT, n = 2) compared to SG (n = 5 – 6). Supervised clustering was performed using previously defined ILC1 versus NK cell signature genes [S1]. Data are combined from 2 independent experiments. (**C – D**) Transcription factors required for the development of ILC1, sgNK and NK cells were examined in SG and liver using mixed bone marrow chimera from WT (CD45.1) and congenically distinct mice (CD45.2) lacking (**C**) *Tbx21* or (**D**) *Eomes* (*Ncr1*^{cre}*Eomes*^{flox}). Data are shown as relative chimerism of the KO (CD45.2) to WT (CD45.1) ratio of lymphocyte populations normalized to the ratio of control WT (CD45.1) and WT (CD45.2) reconstituted bone marrow chimera and are pooled from 2 independent experiments (n = 3 – 5 mice per group). (**E**) Parabiotic mice were generated, and the percentage of donor derived cells localized to the liver and SG determined. The % donor derived cells localized to the tissues was calculated as follows: number of donor derived cells for each of the indicated cell populations/total number of the indicated cell population in the tissue x100. Data are pooled from of 2 independent experiments (n = 3 – 5 mice per group).

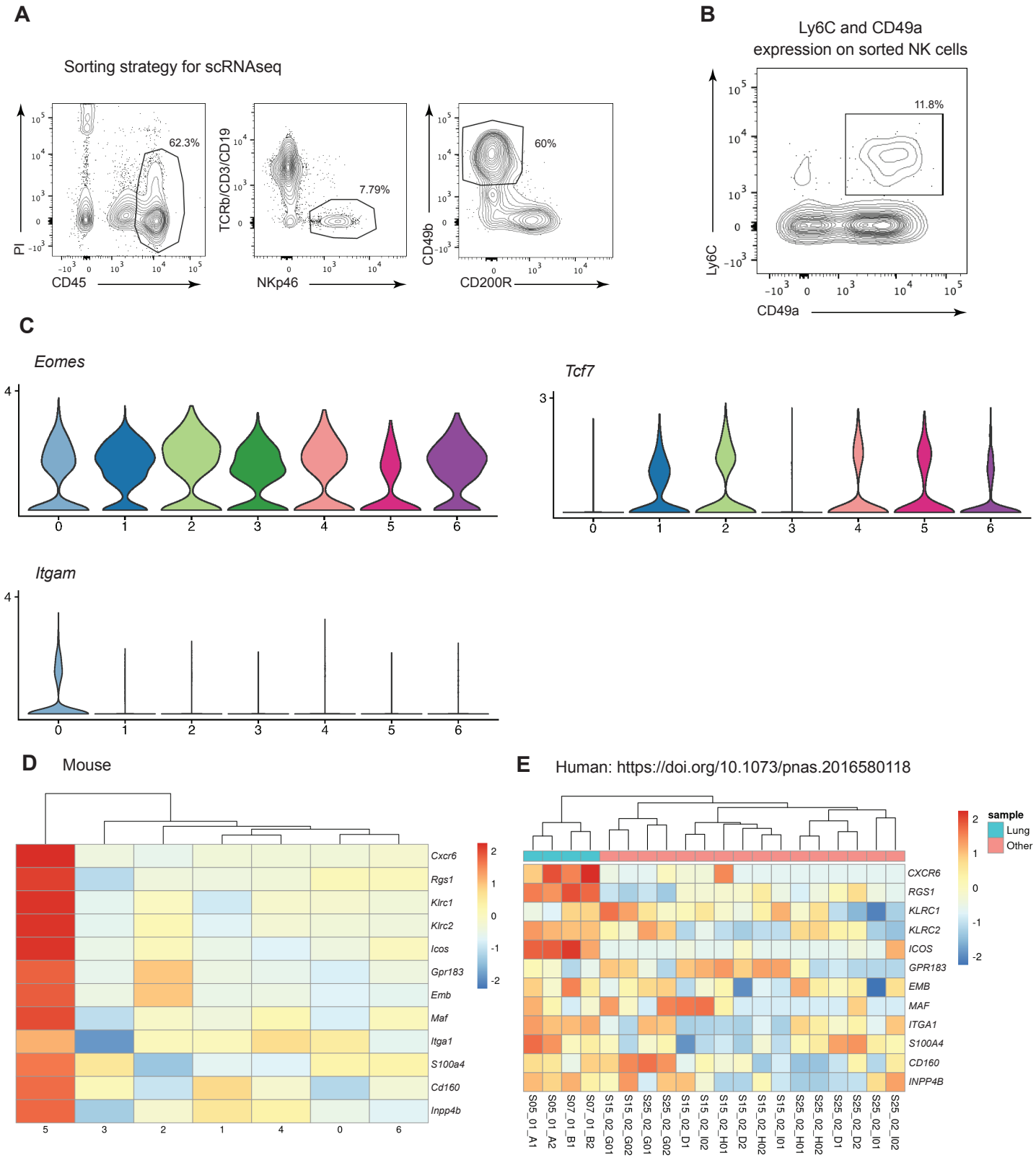

Figure S3. scRNAseq of SG NK cells and shared transcriptional signatures in NKRM and human lung-resident adaptive-like NK cells. Related to Figure 3.

(**A**) NK cells were isolated from the SG of BALB/c mice infected with MCMV (n = 12) on day 120 PI and sorted as live (propodium iodide$^-$) CD45$^+$ TCRb$^-$ CD3$^-$ CD19$^-$ NKp46$^+$ cells that lacked CD200R and expressed CD49b. (**B**) Ly6C and CD49a are co-expressed in a population of the sorted NK cells. (**C**) Violin plots displaying *Eomes*, *Tcf7* and *Itgam* transcripts in scRNAseq clusters. Heat maps of (**D**) genes defining cluster 5 NK cells from SG of MCMV infected mice and (**E**) adaptive-like NK cells with a tissue resident phenotype in human lung and blood [S2].

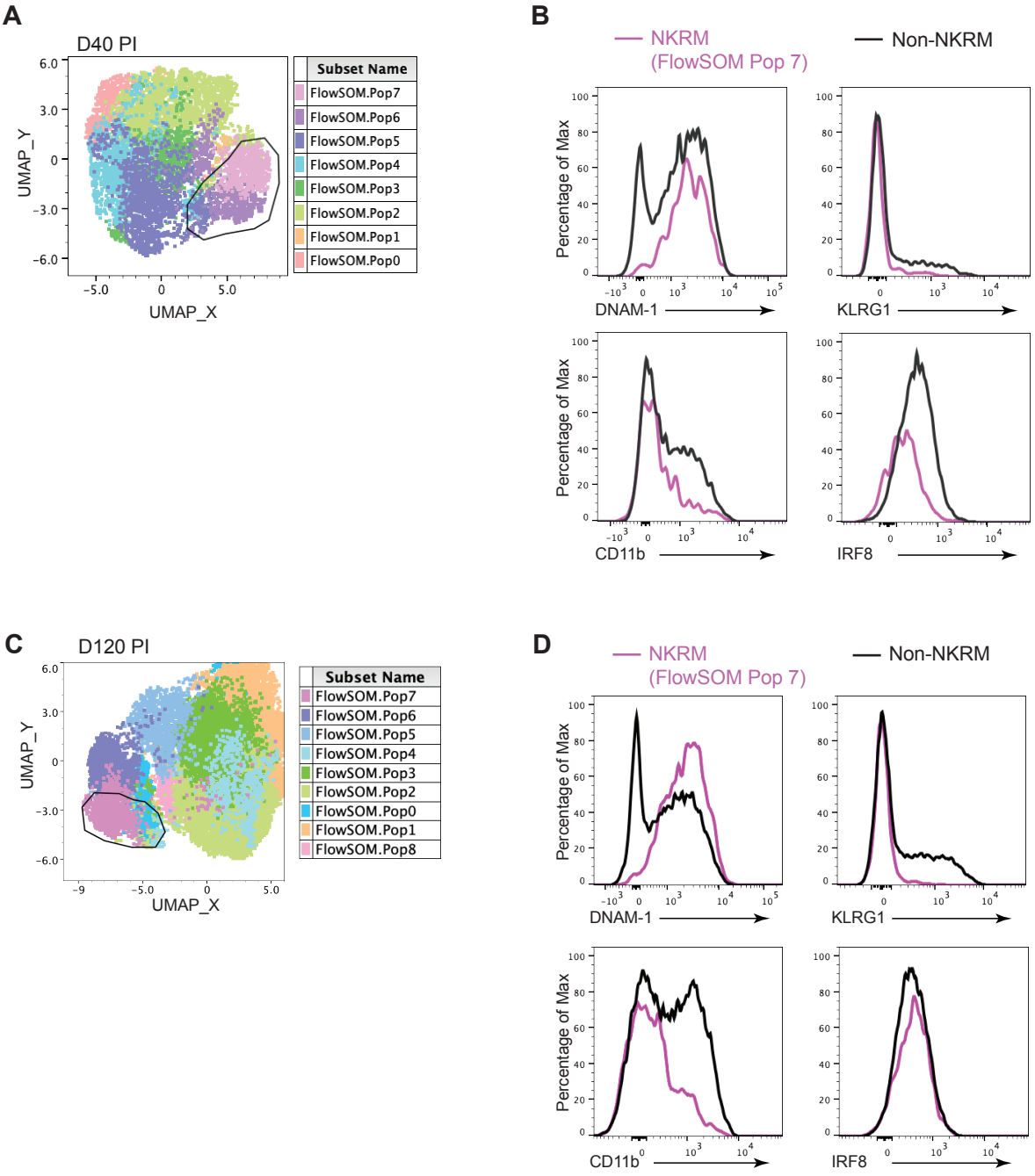

Figure S4. Identification of NKRM in the SG of latently MCMV infected mice. Related to Figure 4.

Overlay of FlowSOM clustered populations onto UMAP analysis of SG NK cells isolated from MCMV infected mice (day 40 PI, **A** – **B** and day 120 PI, **C** - **D**). (**A**) NKRM are localized relative to other populations on the UMAP, which displays the overlayed FlowSOM populations. (**B**) Histograms show the expression of indicated markers in NKRM (FlowSOM population 7) compared to all other NK cells (non-NKRM) in the SG on day 40 PI. (**C**) NKRM are localized relative to other populations on the UMAP, which displays the overlayed FlowSOM populations. (**D**) Histograms show the expression of indicated markers in NKRM (FlowSOM population 7) compared to all other NK cells (non-NKRM) in the SG on day 120 PI. Data are concatenated from n = 5 mice (day 40 PI) and n = 6 mice (day 120 PI) pooled from 2 independent experiments.

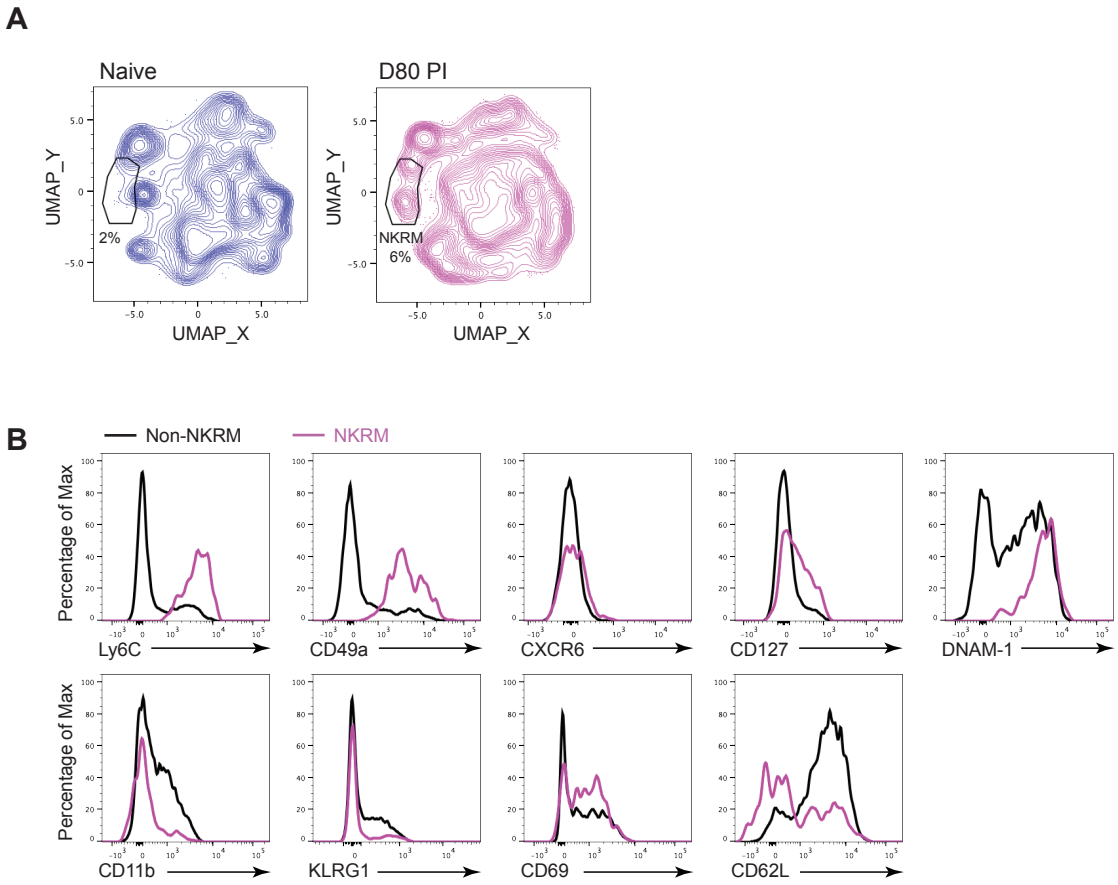

Figure S5. NKRM are present in the lungs of latently MCMV infected but not naïve mice. Related to Figure 4. (**A**) UMAP dimensional reduction analysis of IV$^-$ NK cells (NKp46$^+$CD49b$^+$CD200R$^-$) in the lungs of MCMV infected BALB/c mice. The same parameters used for SG NK cells were applied. UMAP plots of NK cells from naïve mice or MCMV infected mice at day 80 PI. The NKRM gate represents a population present in infected mice. Concatenated data are shown (n = 4 naïve, n = 5 at day 80 PI). (**B**) Histogram overlays show expression of indicated markers in NKRM compared to all other NK cells in the lungs. Data are concatenated from n = 5 mice and representative of 2 independent experiments.

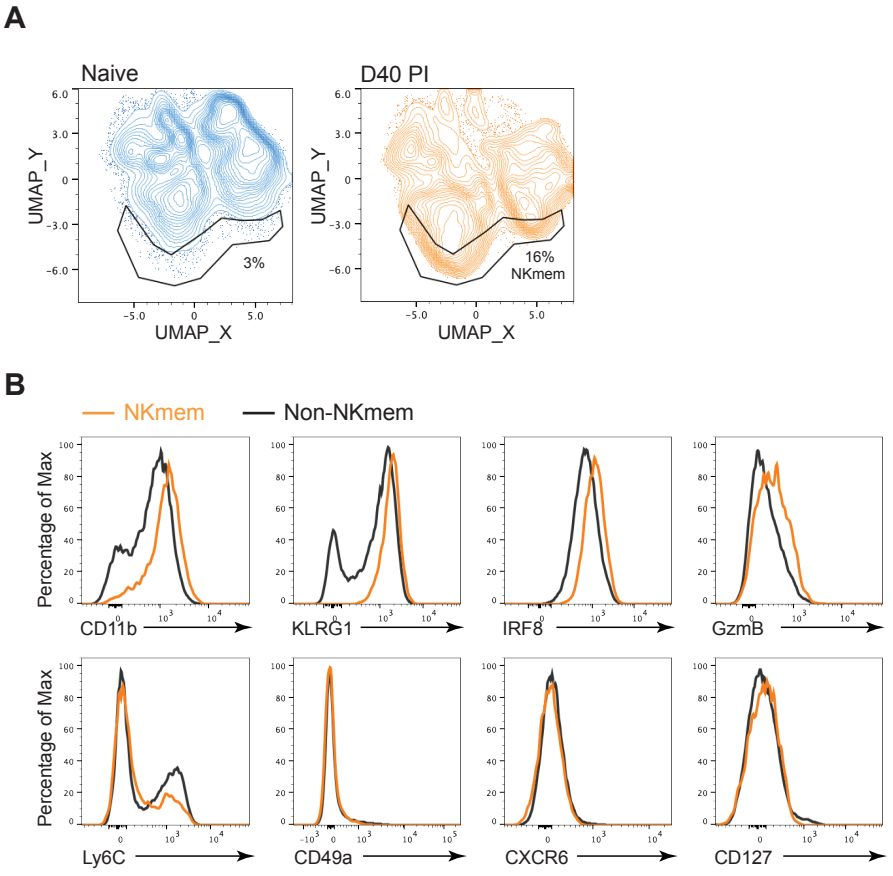

Figure S6. NKRM are absent in the spleen of latently MCMV infected mice. Related to Figure 4.

UMAP analysis of NK cells (NKp46^{+}CD49b^{+}CD200R^{-}) from the spleen of MCMV infected BALB/c mice. The same parameters used for SG NK cells were utilized. (**A**) UMAP plots of NK cell data from naïve mice or MCMV infected mice at day 40 PI. The gate indicates the area that identifies a population present only in infected mice (NKmem). Concatenated data are shown (n = 2 naïve, n = 5 at day 40 PI). (**B**) Histogram overlays compare the expression of indicated markers in NKRM compared to all other NK cells in the spleen. Data are concatenated from n = 5 mice and are representative of 2 independent experiments.

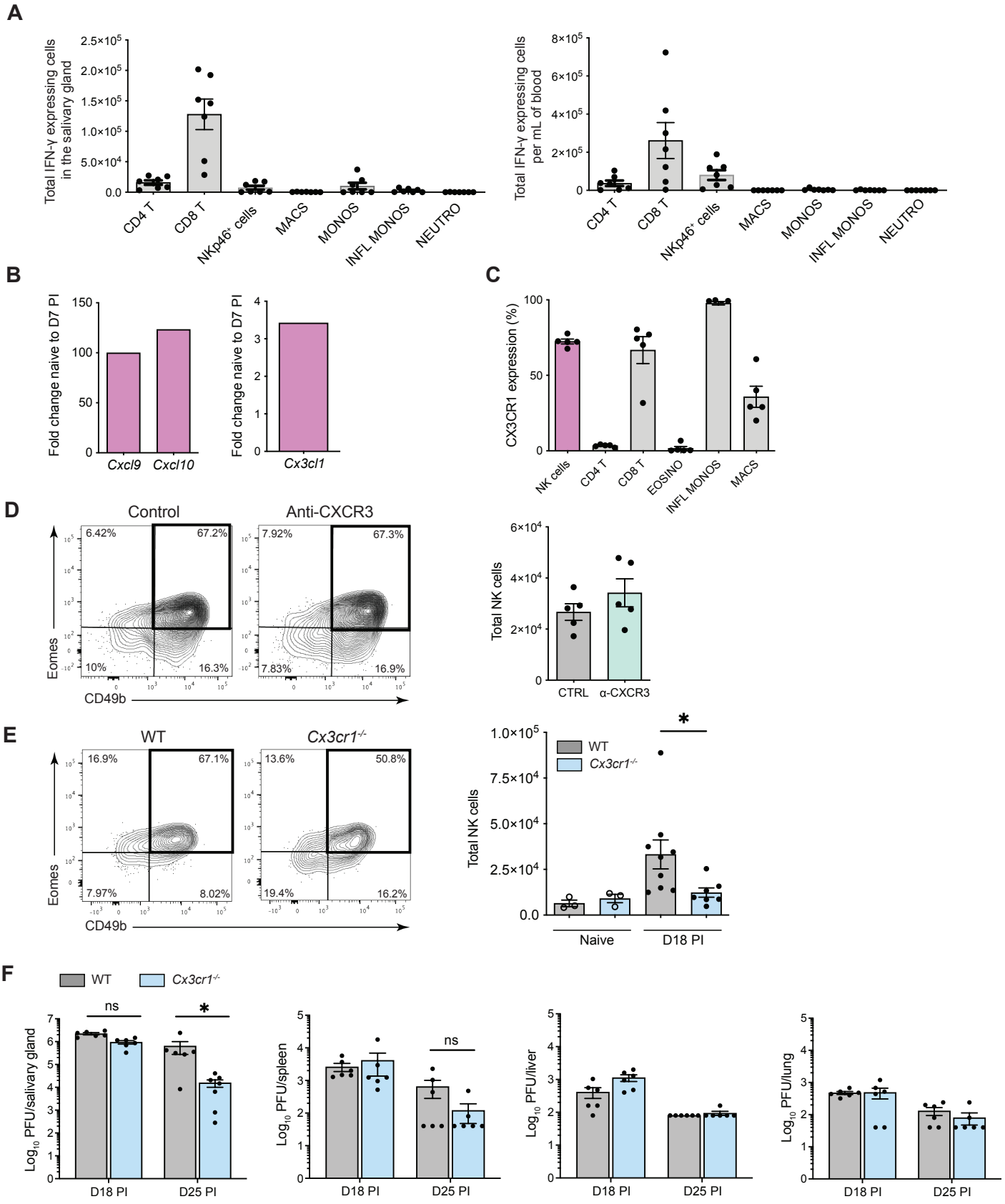
A
Total IFN-γ expressing cells in the salivary gland
2.5×10^5
2.0×10^5
1.5×10^5
1.0×10^5
5.0×10^4
0.0
CD4 T
CD8 T
NKp46+ cells
MACS
MONOS
INFL MONOS
NEUTRO
Total IFN-γ expressing cells per mL of blood
8×10^5
6×10^5
4×10^5
2×10^5
0
B
Fold change naive to D7 PI
150
100
50
0
Cxcl9
Cxcl10
Fold change naive to D7 PI
4
3
2
1
0
Cx3cl1
C
CX3CR1 expression (%)
100
50
0
NK cells
CD4 T
CD8 T
EOSINO
INFL MONOS
MACS
D
Control
Anti-CXCR3
6.42%
67.2%
10%
16.3%
7.92%
67.3%
7.83%
16.9%
Eomes
CD49b
Total NK cells
6×10^4
4×10^4
2×10^4
0
CTRL
α-CXCR3
E
WT
Cx3cr1-/-
16.9%
67.1%
7.97%
8.02%
13.6%
50.8%
19.4%
16.2%
Eomes
CD49b
Total NK cells
1.0×10^5
7.5×10^4
5.0×10^4
2.5×10^4
0.0
*
WT
Cx3cr1-/-
Naive
D18 PI
F
WT
Cx3cr1-/-
ns
*
Log10 PFU/salivary gland
D18 PI
D25 PI
Log10 PFU/spleen
ns
Log10 PFU/liver
Log10 PFU/lung

Figure S7. CX3CR1 is required for the recruitment of NK cells into the SG. Related to Figures 6 and 7. (**A**) BALB/c.*Ifng*$^{-}$YFP reporter mice were infected with MCMV and IFN-γ expressing leukocytes in SG (left) and blood (right) enumerated at day 10 PI. CD4 T (TCRb^{+}CD4^{+}), CD8 T (TCRb^{+}CD8^{+}), NKp46^{+} cells (TCRb^{-}NKp46^{+}), MACS: macrophages (F4/80^{+}), MONOS: monocytes (CD11b^{hi} Ly6C^{-}), INFL MONOS: inflammatory monocytes (CD11b^{hi}Ly6C^{+}) and NEUTRO: neutrophils (Ly6G^{+}). Data are combined from two independent experiments (n = 7). Means ± SEM are plotted. (**B**) qPCR analysis of *Cxcl9*, *Cxcl10* and *Cx3cl1* transcripts in SG homogenates from BALB/c (WT) mice on day 7 PI (shown as fold change relative to naïve, n = 6, pooled from 2 independent experiments). (**C**) Frequency of CX3CR1 expression in blood leukocytes from BALB.*Cx3cr1*-GFP mice on day 18 PI. n = 5, means ± SEM are shown. (**D**) BALB/c were treated with 200µg each of anti-CXCR3 (clone CXCR3-173) and anti-CXCL9 (clone MIG-2F5.5) (α-CXCR3) on days 9, 13 and 17 PI. Representative plots showing frequency of ILC1 (Eomes^{-}CD49b^{-}), sgNK (Eomes^{+}CD49b^{-}) and NK cells (Eomes^{+}CD49b^{+}) and the total number of NK cells in the SG of CTRL or α-CXCR3 treated mice on day 18 PI. Data are plotted as mean ± SEM from n = 5 per group. (**E**) Representative plots showing the frequency of ILC1 (Eomes^{-}CD49b^{-}), sgNK (Eomes^{+}CD49b^{-}) and NK cells (Eomes^{+}CD49b^{+}) and the total number of IV^{-} NK cells in the SG of WT and *Cx3cr1*$^{-/-}$ mice on day 18 PI. Data are plotted as mean ± SEM from n = 7 – 9 per group, pooled from 2 independent experiments. (**F**) Viral loads in WT and CX3CR1-deficient mice, shown as PFU. Data are pooled from 2 experiments and plotted as mean ± SEM for n = 6 –7 mice per group. Statistical analysis performed using a Mann Whitney t test. *p < 0.05.

References

[S1] Weizman, O.E., Adams, N.M., Schuster, I.S., Krishna, C., Pritykin, Y., Lau, C., Degli-Esposti, M.A., Leslie, C.S., Sun, J.C., and O'Sullivan, T.E. (2017). ILC1 Confer Early Host Protection at Initial Sites of Viral Infection. Cell 171, 795-808 e712. 10.1016/j.cell.2017.09.052.

[S2] Brownlie, D., Scharenberg, M., Mold, J.E., Hard, J., Kekalainen, E., Buggert, M., Nguyen, S., Wilson, J.N., Al-Ameri, M., Ljunggren, H.G., et al. (2021). Expansions of adaptive-like NK cells with a tissue-resident phenotype in human lung and blood. Proc Natl Acad Sci U S A 118. 10.1073/pnas.2016580118.